SDC-93-449

SDC
SOLENOIDAL DETECTOR NOTES

INCIDENT ENERGY DEPENDENCE OF HADRONIC ACTIVITY

February 17,, 1993

T.A. Gabriel
Oak Ridge National Laboratory

D.E. Groom
Lawrence Berkeley Laboratory

P.K. Job
ARgonne National Laboratory

N.V. Mokhov
IHEP, Serpukov, Russia and SSCL

G.R. Stevenson
CERN

INCIDENT ENERGY DEPENDENCE OF HADRONIC ACTIVITY

T. A. Gabriel
Oak Ridge National Laboratory, Oak Ridge, TN 37831-6356, USA
D. E. Groom
Lawrence Berkeley Laboratory, Berkeley, CA 94720, USA
P. K. Job
Argonne National Laboratory, Argonne, IL 60439-4815, USA
N. V. Mokhov
IHEP, Serpukov, Russia, and SSCL, Dallas, TX 75237-3946, USA
G. R. Stevenson
CERN, CH-1211 Geneva 23, Switzerland

Two features of high-energy hadronic cascades have been long known to shielding specialists: (a) in a high-energy hadronic cascade in a given material (incident $E \gtrsim 10$ GeV), the relative abundance and spectrum of each hadronic species responsible for most of the energy deposition is independent of the energy or species of the incident hadron, and (b) because π^0 production bleeds off more and more energy into the electromagnetic sector as the energy of the incident hadron increases, the absolute level of this low-energy activity rises less rapidly than the incident energy, and in fact rises very nearly as a power of the incident energy. Both features are of great importance in hadron calorimetry, where it is the "universal spectrum" which makes possible the definition of an intrinsic e/h, and the increasing fraction of the energy going into π^0's which leads to the energy dependence of e/π. We present evidence for the "universal spectrum," and use an induction argument and simulation results to demonstrate that the low-energy activity scales as E^m, with $0.80 \lesssim m \lesssim 0.85$.

1. Introduction

The number of secondaries in a high-energy hadron-induced cascade increases very rapidly as the cascade evolves. In the first few generations π^0's are produced, "bleeding off" a substantial fraction of the energy into electromagnetic cascades. The cascade continues until the final particles lose their energy by such processes as ionization, nuclear excitation, spallation, and fission. Ionization and spallation losses by high-energy particles contribute only negligibly to the total energy deposition, and it is fair to say that essentially all of the energy deposition, activation, neutron yield, *etc.*, are produced by low-energy particles.

The pivotal process in a hadronic cascade is the division of energy between the electromagnetic and hadronic sectors. Except through relatively infrequent process such as neutron photoproduction, the energy carried by the π^0's is not involved with subsequent hadronic processes, and for the purposes of this paper is of concern only in that an average fraction F_{π^0} of the energy disappears from the hadronic sector as the cascade develops. This logic is illustrated in Fig. 1. Note that F_{π^0} is the fraction of the energy carried by π^0's in *all* generations; we will later use f_{π^0} for the average energy fraction carried off by π^0's in a single interaction.

The hadronic sector is defined as everything other than π^0 production, that is, the hadronic energy fraction F_h is defined as $1 - F_{\pi^0}$. It includes energy lost through ionization and spallation by high-energy hadrons, as well as all of the energy carried by hadrons below the π^0 threshold. It includes nuclear binding energy losses. The relatively small amount of electromagnetic energy produced in such processes as (n, γ) reactions is also assigned to the hadronic sector, since this energy fraction is proportional to the hadronic energy. For

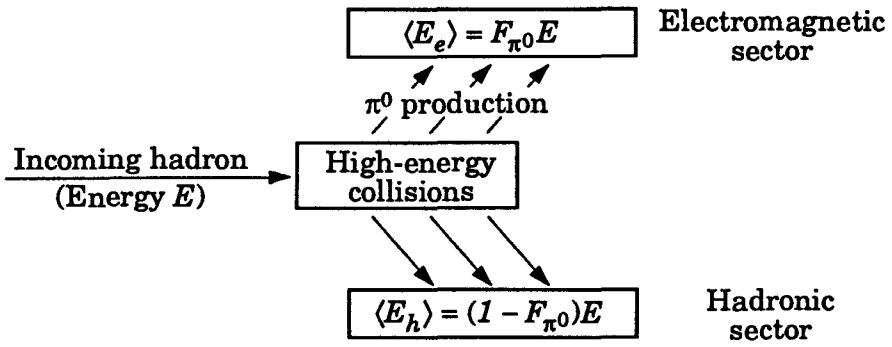

FIG. 1. Logic flow in a hadronic cascade. The energy in the hadronic sector is defined as the energy not going into π^0 production, although a more detailed treatment would exclude energy escaping from the front face of the absorber, energy escaping as neutrinos, and energy deposited after a possible electronic gate. Other than for front-face losses, total containment is assumed.

purposes of the "broad brush" treatment given here, we also include the small amount of energy lost in the form of neutrinos, energy deposited outside of a possible electronic gate, and hadronic loss from the front surface of a calorimeter or beam stop ("albedo losses"), although such losses can be included without much additional complication.

For simplicity we also assume that the cascade is completely contained in a uniform medium, where by "uniform" we mean "uniform over a neutron mean free path." Examples include concrete blocks, soil, and calorimeters consisting of alternating layers of absorber and readout material.

We shall first examine the extent to which the relative abundance and spectrum of each hadronic species is independent of the origin of the cascade, and then explore the energy dependence of F_h.

2. The universal low-energy hadron spectrum

A small number of high-energy secondary particles (mostly pions) and spallation products are produced in the first collision of a high-energy primary hadron incident on a calorimeter or other "beam stop." The secondary π^0's decay, and the other high-energy hadrons undergo subsequent inelastic collisions. The number of interactions ("stars") increases rapidly as the particle energy degrades. Most of the activity, and in fact most of the energy deposition, occurs at low energies, and to the extent that this is true, all information about the origin of the cascade is lost. Although the level of activity varies with the energy of the incident hadron, the energy distribution and relative importance of each hadronic species is independent of incident species or energy.

The "universal spectrum" concept has been known for many years, mostly in connection with radiation shielding problems [1]. The results of a MARS10 simulation are shown in Figs. 2 and 3.* Fig. 2 shows neutron spectra (averaged over the cascade) produced by 10,

* The quantity $d\phi/d\ln E = E\,d\phi/dE$ is called the *lethargy spectrum* by radiation physicists, but it is widely used to describe such quantities as differential cross sections when a logarithmic scale on the horizontal axis is used. Its advantage is that if the vertical scale is linear, the area under the curve is the integral of $d\phi/dE$.

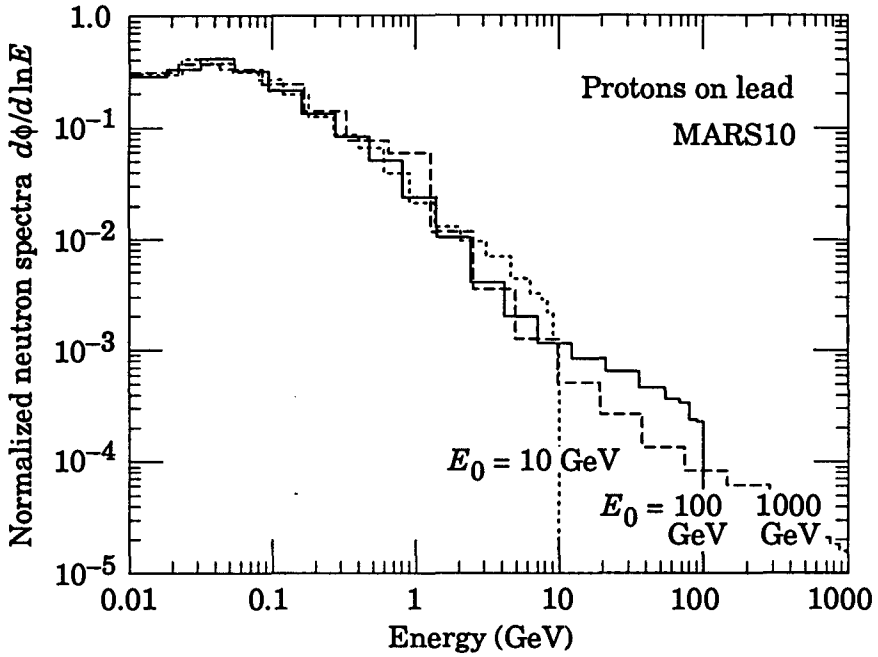

FIG. 2. MARS10 simulations of the neutron spectra in a lead beam stop for incident proton energies of 10, 100, and 1000 GeV. Spectra are for all of the neutrons in the cascade. They are normalized for relative agreement at low energies to emphasize the shape identity below the beam energy cutoff.

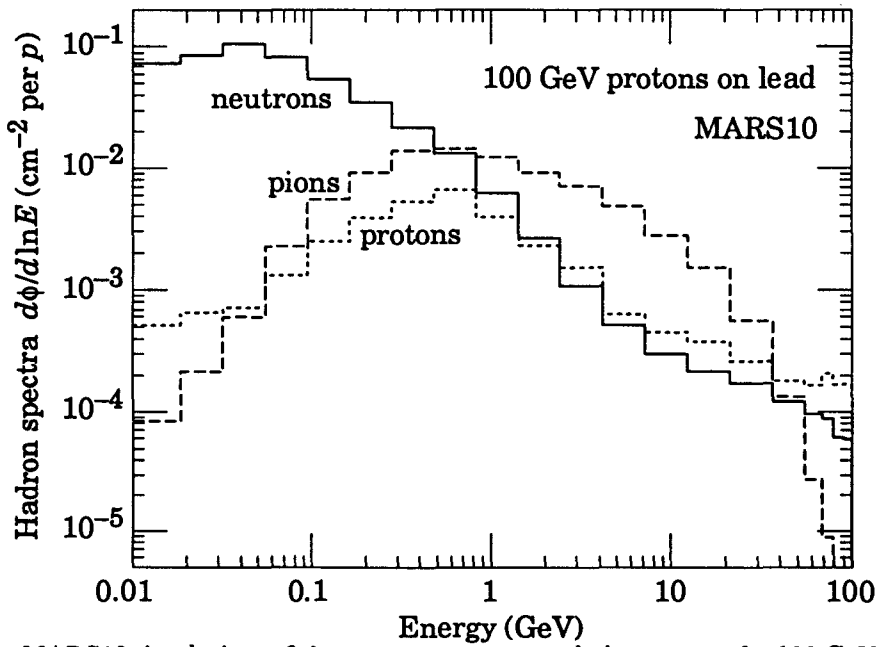

FIG. 3. MARS10 simulations of the neutron, proton, and pion spectra for 100 GeV incident protons on lead. At low energies the charged particles are removed by ionization loss. At high energies the neutrons and protons have similar spectra. In this case there is no normalization. The relative numbers, particularly of neutrons, will be different in a different material.

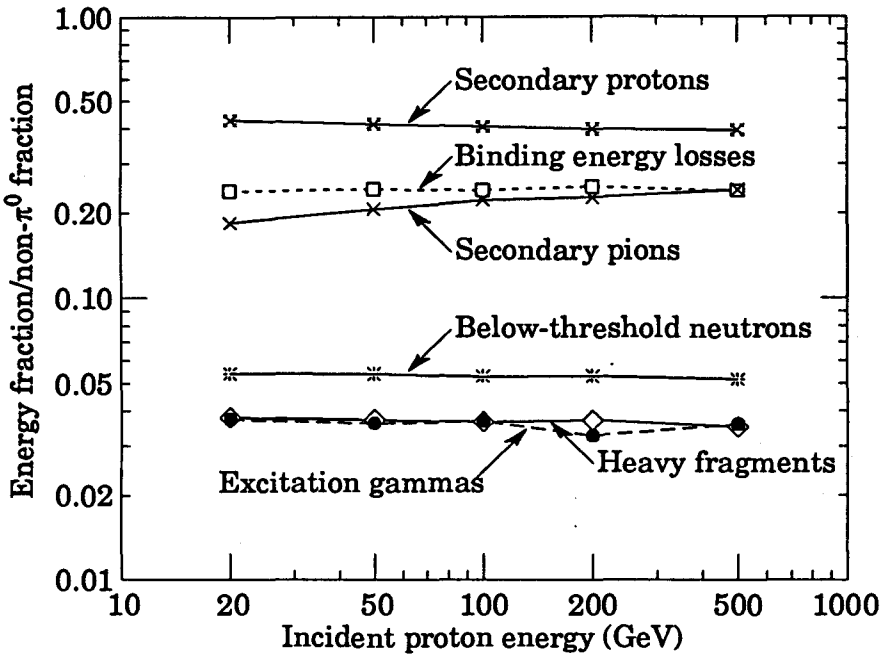

FIG. 5. Hadronic energy loss by various mechanisms in cascades initiated by protons in aluminum, as simulated with HETC. Energy deposits are given as fractions of the energy not converted to π^0's. Not shown is ionization energy loss by the incident proton, which is constant at about 0.23 GeV; this amounts to 1.6% of the hadronic fraction at 20 GeV and 0.1% at 500 GeV.

20 and 500 GeV, in exchange for a decrease in the secondary proton energy deposit from 43% to 39% of the hadronic energy.

In hadron calorimetry, the sampling efficiencies are in general different for the electromagnetic and hadronic components of the deposited energy. These efficiencies (e and h, respectively),* as obtained from CALOR89 [6,7] simulations, are given in Table 1 for four uniform calorimeter configurations with incident π^- energies ranging from 25 to 227 GeV. The constancy of h for each configuration provides further evidence for the energy-independence of the hadronic spectra. Since e is also constant (calorimeters normally have linear response to electrons), the ratio e/h is also constant. Were it not for the "universal spectrum," an intrinsic e/h could not be defined.

Of course the "universal spectrum" theorem is not quite true. We have already discussed the change in the proton/pion ratio shown in Fig. 5. A higher-energy primary is capable of producing more high-energy secondaries, but these contribute little to the total energy deposition. Moreover, there are a variety of geometrical effects. The higher-energy

* Although it is the ratio of e and h which is usually encountered, it is useful to refer these sampling fractions to the sampling fraction of the active medium for a minimum ionizing particle. For example, suppose an ensemble of minimum ionizing particles lose 100 GeV in the "2.54 cm Lead" calorimeter of Table 1. Since $e = 0.60$, we would expect a signal only 0.60 as large from the cascade of a 100 GeV photon. In both cases, only a small fraction of the energy is actually deposited in the readout layers, which in this case is plastic scintillator.

100, and 1000 GeV protons striking solid lead, all normalized for relative agreement at low energies [2]. Almost all of the particles have energies below 1 GeV, even for a 1 TeV incident beam, and the shapes of the spectra (below cutoffs set by the incident beam energies) are identical within the accuracies of the simulations. There may be some excess in the decade just below the cutoff energy.

Fig. 3 shows spectra for the three main hadronic species, this time for an incident proton energy of 100 GeV. As might be expected, the high-energy proton spectrum is about the same as that of neutrons. At low energies the protons quickly lose energy by ionization. They are nearly two orders of magnitude less important than neutrons at 100 MeV and vanish rapidly as the energy decreases. Charged pions have a similar behavior, but they are more abundant than nucleons at high energies.

With proper transport to lower energies, the neutron spectrum shows a broad peak with its maximum just below 1 MeV [3]. For example, Fig. 4 shows HETC88 simulations of the neutron flux at 0.875 TeV and 20 TeV produced by beam-gas collisions in the Tevatron tunnel [4,5]. The 20 TeV flux has been scaled downward for comparison of the spectral shapes. Experimental measurements of the neutron spectrum at 900 GeV are in very good agreement with the simulation results.

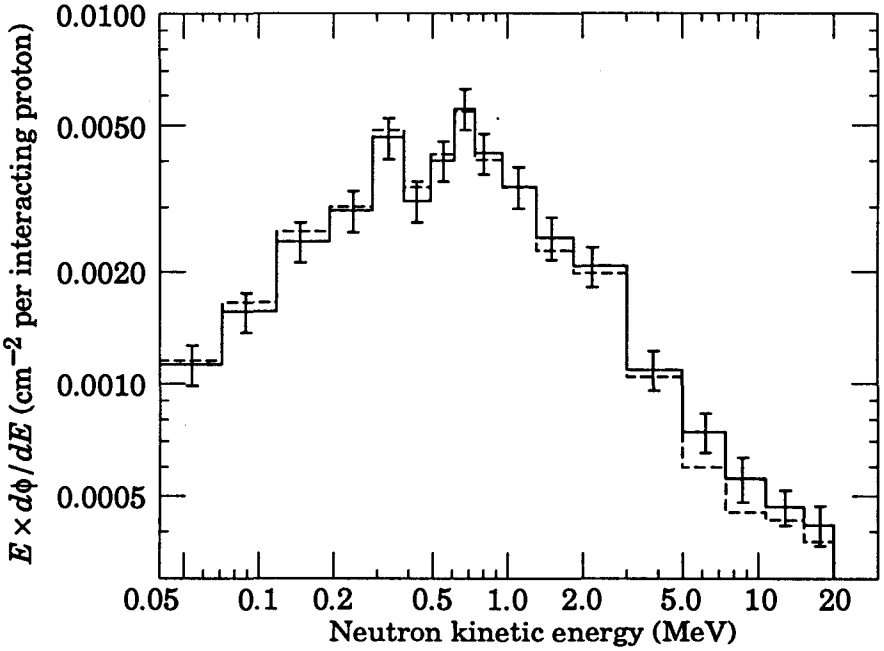

FIG. 4. Neutron spectra at 875 GeV and 20 TeV in the Tevatron tunnel. The solid histogram is an HETC/MORSE simulation at 875 GeV, and the dashed histogram is a simulation at 20 TeV, normalized to emphasize the identity of the spectral shapes.

In Fig. 5 we show the various fractional contributions to energy in the hadronic sector, this time simulated with HETC [6] for protons incident on an aluminum cylinder. To the extent that the mix of low-energy hadronic components is independent of energy, each component should be a constant. There is actually some energy dependence. The fraction of hadronic energy deposited by secondary charged pions increases from 18% to 24% between

secondaries and spallation nucleons tend to concentrate nearer the axis and nearer the beginning of the cascade. Only neutrons propagate to large radial distance from the shower core, and low-energy neutrons (below ~150 MeV) have a flatter radial distribution than do higher-energy components [8]. Such effects could be important in some situations, such as activation near the cylindrical surface of a beam stop. However, in situations ranging from shielding to calorimetry, there is a certain amount of averaging over the cascade geometry, and the spatial variations tend to average out.

Table 1

CALOR89 [7] simulation values for e and h for four calorimeter configurations. Each of the identical cells in each configuration consists of a 100 cm × 100 cm absorber plate as specified, followed by a 0.3 cm plate with the same transverse dimensions. In the two 2.54 cm plate configurations there are 68 cells. For the 1.90 cm configurations there are 92 cells in the lead case and 90 cells in the iron case. The arbitrary normalizations of e and h are chosen in this case relative to the sampling efficiency for minimum ionizing particles.

E_{π^-} (GeV)	2.54 cm Lead		1.90 cm Lead		2.54 cm Iron		1.90 cm Iron	
	e	h	e	h	e	h	e	h
25	0.601	0.704	0.603	0.674	0.852	0.578	0.854	0.555
50	0.602	0.708	0.605	0.670	0.850	0.576	0.858	0.552
100	0.599	0.703	0.605	0.677	0.851	0.563	0.858	0.559
150	0.603	0.703	0.603	0.677	0.855	0.561	0.857	0.545
227	0.602	0.703	0.605	0.678	0.857	0.569	0.855	0.543
Average	0.601	0.704	0.604	0.675	0.853	0.569	0.856	0.551

3. "Low-energy hadronic activity"

There are many measures of "low-energy hadronic activity," all of which exhibit almost the same dependence on incident hadron energy. These include:

1. Number of nuclear interactions ("stars") produced in the absorber by hadrons whose energy exceeds some threshold E_t. Most such interactions are induced by hadrons (usually neutrons) with energies not far above E_t, and the comparatively few interactions with $E > E_t$ contribute little to the total. This measure has the advantage of being easily tallied by the transport code, and it is readily available. This and other code-produced quantities are shown in Fig. 6; other examples are shown in Fig. 5.
2. The yield of a given radionuclide; *e.g.* ^{54}Mn in an iron absorber, ^{60}Co in stainless steel, or ^{239}Np in a uranium calorimeter [9].
3. The hadronic part of calorimeter response. The total response is a combination of electromagnetic response (to the π^0 decay photons) and to the predominately low-energy hadronic activity, but these can be separated by analyzing the energy dependence of the calorimeter's response to incident hadrons.

4. Heuristic derivation of energy dependence

A simple induction argument may be used to obtain the energy dependence of the low-energy hadronic activity. Let $N(E)$ be one of the measures of this activity discussed above; to fix ideas let it be the average number of nuclear stars produced by cascade particles

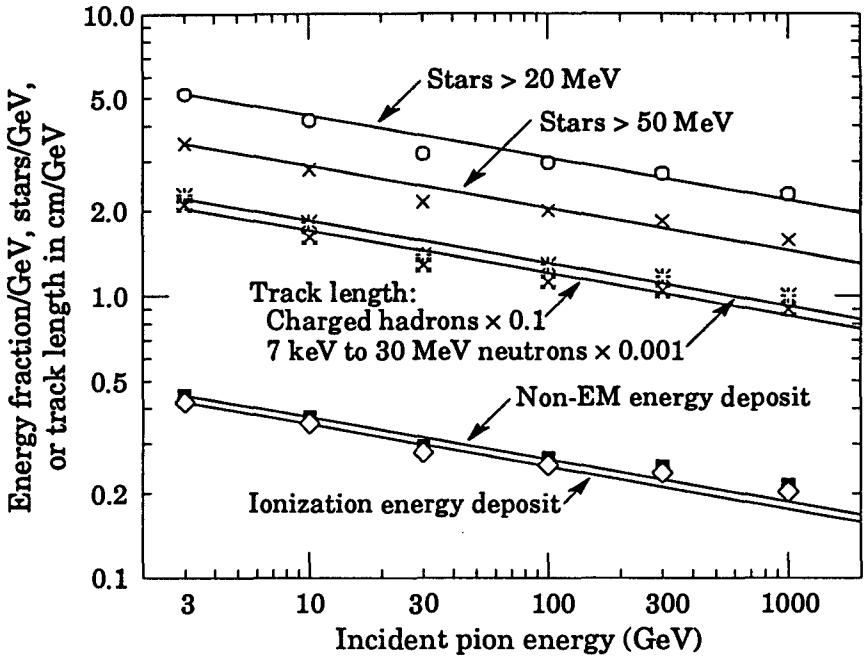

FIG. 6. Measures of hadronic activity simulated with FLUKA92 for protons incident on an iron cylinder. Of particular importance is the number of nuclear interactions (stars) produced by hadrons with energy above some cutoff, here 20 MeV and 50 MeV, and the hadronic energy fraction (non-electromagnetic energy fraction). The former can be related to radionuclide production, and the latter to calorimeter response. Note that the *deposited* hadronic energy (non-EM energy) rather than *total* hadronic energy is plotted. The solid lines have a slope of −0.15.

with energies above E_t in a cascade initiated by a hadron with energy E (the hadron may already be a secondary in a larger cascade). Now consider the activity $N(nE)$ produced by a hadron with energy nE, where n is a multiplier roughly identified with the average multiplicity of high-energy secondaries (charged and neutral) produced in its first collision. Unless it is a π^0, a secondary with energy E_i produces activity $N(E_i)$, and

$$N(nE) = \sum_{\text{daughters}(\neq\pi^0)} N(E_i) \,, \tag{1}$$

where the sum is over secondary particles exclusive of π^0's. Now let us replace the correct sum of activity contributions with the available energy fraction times an average contribution:

$$N(nE) \approx (1 - f_{\pi^0})\, n\, N(E) \tag{2}$$

Here a fraction of the energy f_{π^0} is lost to the hadronic sector through π^0 production. (We distinguish f_{π^0}, the fraction of the energy going into π^0's in one collision, from F_{π^0}, the energy fraction going into π^0's in all the generations of the cascade.) The cascade process as we are modeling it here is shown schematically in Fig. 7.

Insofar as n and f_{π^0} can be treated as constants, the solution to this iterative equation

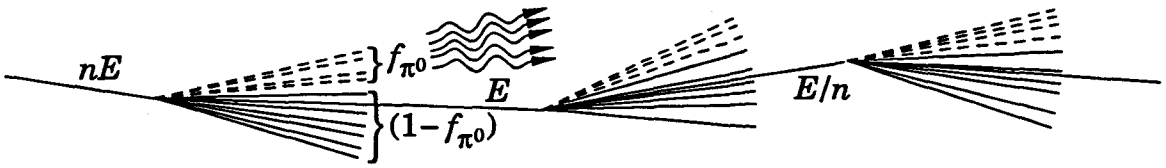

FIG. 7. Schematic of cascade. It is assumed that in each generation the average energy of the cascade particles decreases by a factor n and that an average fraction f_{π^0} of the energy leaves the hadronic sector via π^0 production.

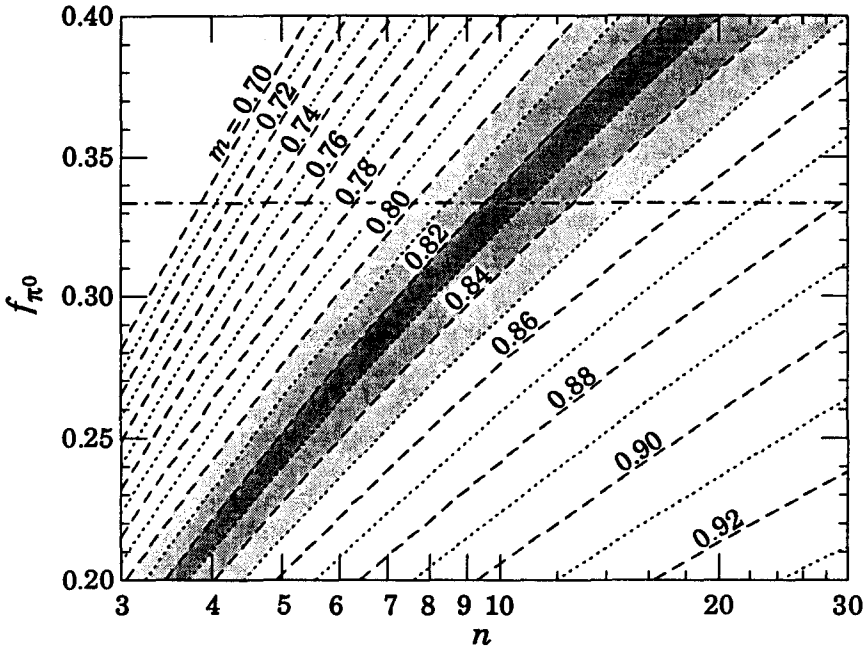

FIG. 8. The average fraction of the energy entering the electromagnetic sector f_{π^0} as a function of the average total multiplicity n for a single high-energy collision in a cascade for fixed values of the power m, as given by Eq. (4). Estimates of m from the most dependable simulations fall in the shaded region. One expects $f_{\pi^0} \lesssim 1/3$.

is a power law,

$$N(E) = K\,E^m\ , \tag{3}$$

with

$$1 - m = \frac{\ln\left(1/(1-f_{\pi^0})\right)}{\ln n}\ . \tag{4}$$

The other assumptions can be discussed most easily after examining the range of the variables. For the choices $f_{\pi^0} = 1/3$ and $n = 20$, we find $m = 0.86$. Halving the multiplicity reduces m to 0.82, and if $f_{\pi^0} = 1/4$ rather than $1/3$, m increases from 0.86 to 0.90. It is difficult to find realistic parameters for which m falls outside the range 0.82 to 0.90. Contours of fixed m are shown as functions of n and f_{π^0} in Fig. 8.

Equation (2) was obtained by assuming that the sum of activities produced by k ($\approx (1 - f_{\pi^0})n$) particles with different energies E_i could be replaced by k times the activity

produced by one particle with the average energy $E = (\sum_k E_i)/k$. Making use of the power-law solution, we see that this is equivalent to

$$\sum_k E_i^m \approx kE^m \ . \tag{5}$$

However, if only one of the secondary particles carried all of the nonelectromagnetic energy, the left side would be $k^m E^m$, which is smaller than the right side by a factor k^{m-1}. If j particles divided the energy equally ($j \leq k$), then the factor would be $(k/j)^{m-1}$. With $n \approx 10$, the result would be about 30% smaller if only one particle carried all the energy, and 15% smaller if two particles divided the energy equally. A leading hadron tends to carry off about half of the energy, and the fragmentation functions favor very unequal energy division among the remaining cascade particles. As a result, our equal-energy assumption probably overestimates the quantity on the right side of Eq. (1) by 10–20%—if we strictly interpret n as the total multiplicity. In reality, the net effect of our approximation is to reduce the multiplier n by 10–20%. It should be thought of as an energy scale factor between generations rather than as a cascade particle multiplicity.

The remaining issues concern the effect of the energy dependence of n and f_{π^0}, which were implicitly assumed to be constant in the above development. The insensitivity of m to either variable is evident from the above discussion or from Fig. 8. The multiplicity increases only logarithmically with energy, so $\ln n$ varies extremely slowly. Although a very slow growth of m with energy is to be expected, the present data shows no conclusive evidence for the increase.

Similarly, $\ln(1 - f_{\pi^0})$ is insensitive to changes in f_{π^0} over its expected range. If the energy were all carried off by pions, then f_{π^0} would be 1/3 by isospin conservation. The presence of secondary nucleons, π^0's from other sources (*e.g.* isobar decay), and leading hadrons all tend to reduce f_{π^0}, so 1/3 should be taken as an upper limit. Values near 1/3 are supported by the simulations. At low energies (10–20 GeV), where most of the π^0 production should occur in the first collision, F_{π^0} (π^0 production in all generations) is found to be 30%–40%.

Finally, we have assumed that the products of a collision will themselves induce similar collisions. This assumption will break down when the secondaries have energies below the π^0 production threshold. The minimum incident energy for the validity of our argument should thus be about 10 GeV.

It is useful to rephrase the logic: After each collision in a hadronic cascade, only $(1-f_{\pi^0})$ of the energy is available (on the average) for the next generation. This factor is applied every time the energy increases by the multiplicity, which results in a power-law increase in low-energy activity with increasing energy of the incident hadron. Stated differently, every collision is very much like every other collision except for the energy scale. The very nature of the process leads to a power-law-like behavior.

According to Eq. (3), the level of low-energy hadronic activity is *proportional* to E^m. We can fix the proportionality constant by a dimensional argument:

$$\begin{aligned} E_h &= E_0(E/E_0)^m \\ &= E(E/E_0)^{m-1} \end{aligned} \tag{6}$$

Here E_0 is a scale energy which should correspond to the energy at which π^0 production has becomes important, or about 1 GeV. The average hadronic energy fraction F_h in a collision is E_h/E, or

$$F_h \equiv (1 - F_{\pi^0}) = (E/E_0)^{m-1} \ . \tag{7}$$

Understanding E_0 as an effective π^0 cutoff energy provides yet another way to obtain our expression for m. The previous cascade generation was induced by hadrons with average energy nE_0, *etc.*, so if there were n_g generations, $E = n^{n_g}E_0$, or $E/E_0 = n^{n_g}$. In each generation F_h is reduced by the factor $(1 - f_{\pi^0})$, so

$$F_h = (1 - f_{\pi^0})^{n_g} = n^{(m-1)n_g} \ . \tag{8}$$

From the relationship $(1 - f_{\pi^0}) = n^{(m-1)}$ one immediately recovers Eq. (4).

5. Comparison with Monte Carlo simulation results

According to the above discussion, every measure of hadronic activity should scale as the same power of the incident energy—at least in a given simulation. Such results are shown in Fig. 6, where lines with slope $m - 1 = -0.15$ provide a good description for all of the data.

A series of FLUKA [10] runs was used to investigate the details of the distribution of the electromagnetic energy fraction on an event-by-event basis in a solid lead beam stop [11]. The behavior of the first moment of the distribution, plotted as $1 - F_{\pi^0}$, is shown in Fig. 9. A least-squares fit of Eq. (7) yields $m = 0.87$ and $E_0 = 0.76$ GeV. There is a little evidence for curvature, as might be expected from the slow increase of multiplicity with energy, but this is not corroborated by other studies reported here.

Similar results are shown in Fig. 10 for two sandwich calorimeters simulated with CALOR89 [6,7] (these are two of the runs for which e and h are reported in Table 1.) This time the best-fit power is somewhat smaller, about 0.83 for both lead and iron. The difference appears to reflect π^0 production differences between the two codes. In the lead case $E_0 = 1.3$ GeV, and for iron it is 0.7 GeV, reflecting a 5% smaller hadronic activity (fewer neutrons) in iron than in lead.

A value of the power for higher energies from HETC/MORSE comparisons of the expected neutron flux at the Tevatron and SSC, which were run at 20 TeV and 875 GeV [4]. The ratio of longitudinally integrated neutron fluxes was 14.0 for the direct flux and 13.7 with the inclusion of albedo flux, corresponding to $m = 0.84$ in both cases. This is in good agreement with lower-energy HETC results, and argues that m does not decrease much with increasing energy.

These and other simulation results are summarized in Table 2. The actual hadronic fraction is fairly insensitive to the value of E_0, since it is always raised to a very small power $(1 - m \approx 0.13)$. Doubling E_0 produces only an 9% change in F_h. Moreover, m and E_0 are highly correlated. For this reason we also list F_h at 100 GeV, which is near the centroid for the fits. The range of the power m given in Table 2 is 0.78 to 0.87. The lower value is probably errant because of poor statistics at the highest-energy point, and the value 0.87 was obtained with an older version of FLUKA. In the context of the present studies, we conclude $0.80 \lesssim m \lesssim 0.85$.

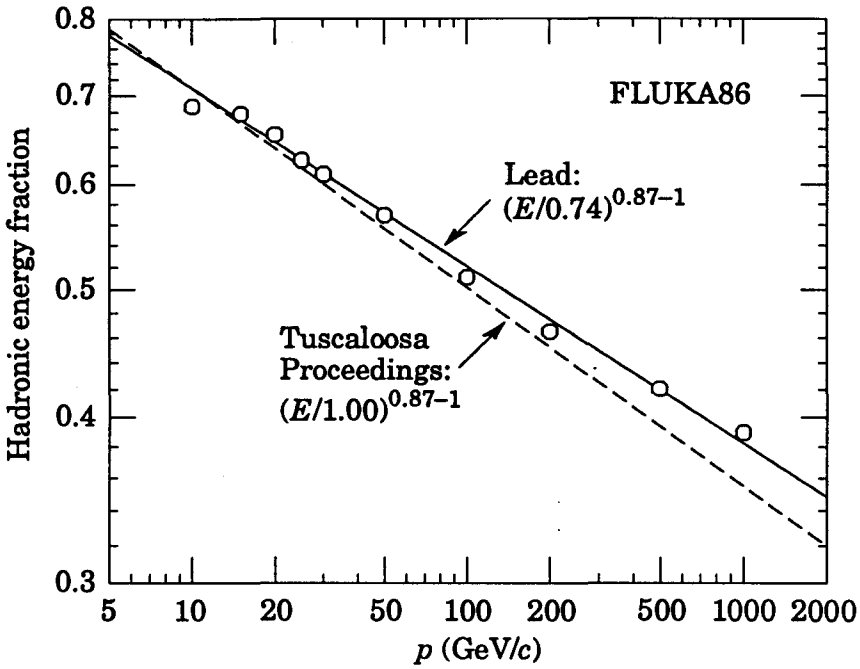

FIG. 9. The mean hadronic fraction F_h as simulated with FLUKA86 for negative pions incident on a lead target. The least squares fit of the function $(E/E_0)^{m-1}$ yields $m = 0.87$ and $E_0 = 0.74$ GeV, shown by the solid curve. The dashed curve is from a preliminary report, assuming $m = 0.85$ and $E_0 = 1.0$ GeV [12].

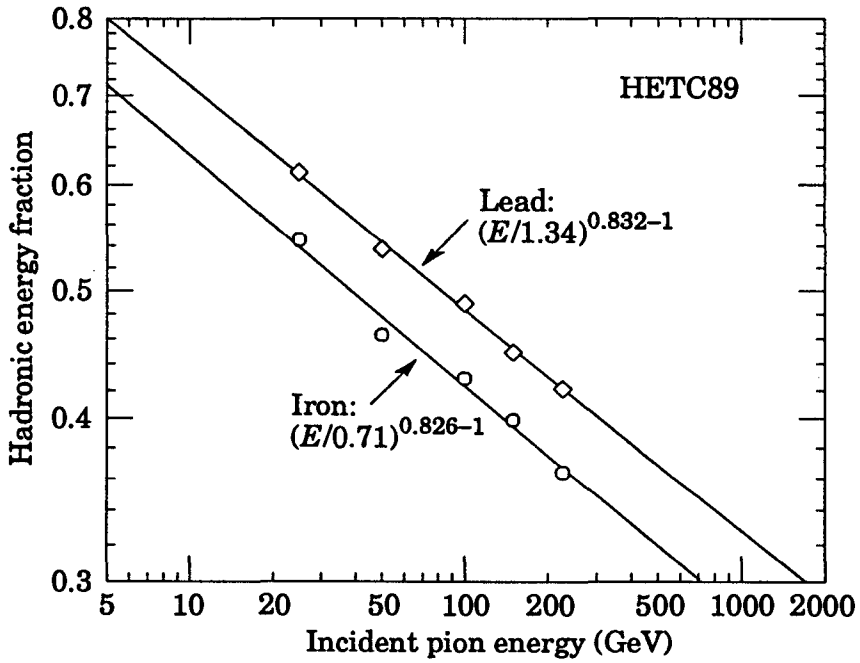

FIG. 10. The mean hadronic fraction F_h as simulated with HETC89 for negative pions incident on a sandwich calorimeter. Each 100 cm × 100 cm cell of the calorimeter consist of 2.54 cm thick metal plate and 0.30 cm plastic scintillator. Other data from the same runs are shown in Table 1.

Table 2

Values of m and E_0 for the hadronic fraction $F_h = (E/E_0)^{m-1}$. The variation of m shown in the table is considered excessive, and is not yet understood. Because E_0 is highly correlated with m, the quantity $F_h(100\text{ GeV}) = (100\text{ GeV}/E_0)^{m-1}$ is also given.

Code	Material	Incident particle	Energy (GeV)	Power m	Scale E_0 (GeV)	F_h at 100 GeV	Comments
FLUKA86	Lead	π^-	10–1000	0.87	0.74	0.53	Cylinder
FLUKA92	Iron	p	3–1000	0.80	*	*	Cylinder
FLUKA92	Iron	π^-	3–1000	0.85	*	*	Cylinder
FLUKA92	Aluminum	π^-	3–1000	0.85	*	*	Cylinder
HETC	Lead	π^-	25–227	0.83	1.34	0.48	Hanging file calorimeter
HETC	Iron	π^-	25–227	0.83	0.71	0.43	Hanging file calorimeter
HETC	Aluminum	p	10–1000	0.81	1.54	0.45	Cylinder
HETC	Concrete	p	10–1000	0.78	2.05	0.43	Cylinder
HETC	Tevatron	p	875–20000	0.84	—	—	Full tunnel simulation

* Slope based on *deposited* hadronic energy, so E_0 and $F_h(100\text{ GeV})$ are not available.

It should be emphasized that the division into hadronic and electromagnetic sectors is complete when all particles have fallen below the π^0 threshold, and all of the details of this analysis can be learned without any particle transport below this threshold.

Further studies are needed to resolve (a) differences between materials, if any, (b) why codes give such different results, and (c) whether m and E_0 are sensitive to incident particle species. These will be made before this paper is submitted for publication in a journal. There is, in fact, a physical reason why the power might be different for incident protons than for pions: A large fraction of the energy in a collision is carried by a leading particle, which is a nucleon in the case of a nucleon collision and pion in the case of a pion collision. If it is a pion, then 1/3 of the time it should emerge as a π^0, remove a large fraction of the collision energy from the hadronic sector. In this case m should then be smaller, and $F_h(100\text{ GeV})$ should be smaller. In the two FLUKA92 studies summarized in Table 2, the change in m is in the opposite direction, and the F_h curves cross.

6. Previous work

The power-law growth of hadronic activity is hardly a new idea. In shielding discussions it is related to the source strength parameter in the Moyer model, which is related to multiplication in cascades. Thomas and Stevenson credit the power law to Lindenbaum [13], although it is not in the reference they cite [14]. Lindenbaum suggests $m \approx 0.5$. Thomas and Thomas use later studies to conclude $m = 0.80 \pm 0.10$ [15], and others have extended the range of applicability to higher energies [16,17]. In any event, they do not go beyond the confines of the Moyer model, and Thomas and Stevenson elsewhere assume that neutron yield is proportional to incident energy to ensure an overestimate of hazard.

In a 1972 paper, O'Brien noted that the number of stars divided by the incident energy could not be constant, but must decrease with increasing energy [18]. The curve he gives in Fig. 1 corresponds to $m = 0.84$, and would have been recognized as a power law had he used a logarithmic vertical axis. The lack of energy dependence in the Monte Carlo data

shown in the figure reflects insufficient π^0 production in the early transport codes. O'Brien was aware of the Moyer model work at Lawrence Berkeley Laboratory, but evidently no paper was published supporting the assertion that neutron production, for example, grew as a power of the incident energy [19].

7. Discussion

We have made two points: (a) the concept of low-energy hadronic activity with little memory of its origins is fundamental to studies of shielding, radioactivation, and calorimeter response, and (b) the very nature of the cascade process is such that the level of the hadronic activity scales very nearly as a power of the incident energy: Activity $\propto E^m$.

The exponent m seems to lie in the range 0.80 to 0.85, depending on the Monte Carlo code used to study it and not depending strongly on the material in which the cascade occurs. Since every collision is very much like every other collision, it is possible to obtain an estimate of the exponent by means of an induction argument. The exponent is a function of the average π^0 energy fraction and multiplicity of high-energy secondaries in a single hadron-nucleus collision.

The hadronic energy fraction in a cascade, defined as the energy not transferred to the electromagnetic sector by π^0 production, is given by $(E/E_0)^{m-1}$, where E_0 is a scale factor close to 1 GeV. It is larger for lead than for iron, reflecting the fact that at a given incident energy a larger fraction is lost to nuclear processes for heavier, less tightly bound nuclei.

The asymptotic behavior of the hadronic fraction cannot be overemphasized. Since the exponent m is of necessity less than one, the hadronic fraction slowly approaches zero as the energy increases. This feature is well known in cosmic-ray physics, where the energy deposition in energetic air showers is predominantly electromagnetic. For calorimetry it means that the asymptotic response to a pion is the same as that for an electron: $e/\pi \rightarrow 1$, and the hadronic response is asymptotically linear.

Acknowledgments

This work was supported by the U. S. Department of Energy and by the management of CERN. Although we are indebted to many coworkers for discussions of the ideas and the codes, we especially acknowledge the help of A. Ferrari, T. Handler, and J. Ranft.

References

1. T. A. Gabriel and R. T. Santoro, "Calculation of the Long-Lived Activity in Soil Produced by 500 GeV Protons," Oak Ridge National Laboratory Report ORNL-TM-3262 (1970).
2. N. V. Mokhov, J. D. Cossairt. Nucl. Instrum. Methods, A244 (1986) 349;
   N. V. Mokhov, Soviet J. Particles and Nuclei (Sept.-Oct. 1987) 408-426;
   N. V. Mokhov, "The MARS10 Code System: Inclusive Simulation of Hadronic and Electromagnetic Cascades and Muon Transport," Fermilab Report FN-509 (20 March 1989).
3. "Radiation Levels in the SSC Interaction Regions," ed. D. E. Groom, SSC Central Design Group Report SSC-SR-1033 (June 1988).
4. T. A. Gabriel, F. S. Alsmiller, R. G. Alsmiller, Jr., B. L Bishop, O. W. Hermann, and D. E. Groom, "Preliminary Simulation of the Neutron Flux Levels in the Fermilab Tunnel and Proposed SSC Tunnel," SSC Central Design Group Report SSC-110 (1987).
5. R. G. Alsmiller *et al.*, Nucl. Instrum. Meth. **A313** (1992) 357-366.

6. R. G. Alsmiller, Jr., F. S. Alsmiller, and O. W. Hermann, Nucl. Instrum. Meth. **A295** (1990) 337–343;
F. S. Alsmiller and R. G. Alsmiller, Jr., Nucl. Instrum. Meth. **A278** (1989) 713-721.

7. T. Handler, P. K. Job, L. E. Price and T. A. Gabriel, "Unix Version of CALOR89 for Calorimeter Applications," Solenoidal Detector Collaboration Note SDC-92-257 (1992);
B. R. Moore, "User's Guide to CALOR89-U3G," UMS/HEP/91/016 (1992);
T. A. Gabriel, B. L. Bishop, F. S. Alsmiller, R. G. Alsmiller, Jr., and J. O. Johnson, "CALOR89: A Monte Carlo Program Package for the Design and Analysis of Calorimeter Systems," ORNL/TM-11185 (1993).

8. J. S. Russ, G. R. Stevenson, A. Fassò, M. C. Nielsen, C. Furetta, P. G. Rancoita and L. Vismara, Report CERN/TIS-RP/89-02 (1989);
A. Fassò, G. R. Stevenson, M. Bruzzi, C. Furetta, P. G. Rancoita, P. Giubellino, R. Steni and J. S. Russ, Report CERN/TIS-RP/90-19 (1990);
G. R. Stevenson, A. Fassò, C. Furetta, P. G. Rancoita, P. Giubellino, J. S. Russ and C. Bertrand, Report CERN/TIS-RP/91-11 (1991).

9. C. Leroy, Y. Sirios, and R. Wigmans, Nucl. Instrum. Meth. **A252** (1986) 4.

10. P. A. Aarnio, A. Fassò, H-J. Möhring, J. Ranft and G. R. Stevenson, "FLUKA86 User's Guide," CERN TIS-RP/168 (1986);
P. A. Aarnio, A. Fassò, J. Lindgren, J. Ranft and G. R. Stevenson, "Enhancements to the FLUKA86 Program (FLUKA87)," CERN TIS-RP/190 (1987).

11. D. E. Groom, p. 376 in "Four-Component Approximation to Calorimeter Resolution," *Proc. II Inter. Conf. on Calorimetry in High Energy Physics,* Capri, Italy, 14–18 October 1991, ed. by A. Ereditato, World Scientific (1992).

12. D. E. Groom, "Energy Scaling of Low-Energy Neutron Yield, the e/π Ratio, and Hadronic Response in a Calorimeter," *Proc. of the Workshop on Calorimetry for the Superconducting Super Collider,* Tuscaloosa, Alabama, 13–17 March 1989, ed. R. Donaldson and M. G. D. Gilchriese, World Scientific (June 1990), 59–75.

13. R. H. Thomas and G. R. Stevenson, *Radiological Safety Aspects of the Operation of Proton Accelerators,* Technical Report Series No. 283, IAEA Vienna (1988).

14. S. J. Lindenbaum, Ann. Rev. Nucl. Sci. **11** (1961) 213.

15. R. H. Thomas and S. V. Thomas, Health Phys. **46** (1984) 954.

16. J. D. Cossairt, S. W. Butala, and M. A. Gerardi, Nucl. Instrum. Meth. **A238** (1985) 504.

17. G. R. Stevenson, "Shielding of Extended Targets at Proton Energies of Greater than 3 GeV," CERN Divisional Report TIS/IR/86-04 (1986).

18. K. O'Brien, Nucl. Instrum. Meth. **101** (1972) 551-553.

19. K. O'Brien, private communication (1989).